Analytical Surface for the Reaction with No Saddle-Point $NH_3 + F \rightarrow NH_2 + FH$. Application of Variational Transition State Theory

Joaquín Espinosa-García* and José C. Corchado

Departamento de Química Física, Universidad de Extremadura, 06071 Badajoz, Spain

Received: January 16, 1997; In Final Form: March 21, 1997[⊗]

The title reaction and its deuterated analogue ($ND_3 + F \rightarrow ND_2 + FD$) were studied by means of an analytical expression for their potential energy surface. The analytical form is the one previously used for the similar $NH_3 + H \rightarrow NH_2 + H_2$ reaction. As calibration criteria, we used the reactant and product experimental properties and the theoretically calculated properties of a hydrogen-bonded complex linking NH_2 and FH. Using this potential energy surface, we analyzed the effects of the reaction path curvature (translation−vibration coupling) in order to explain the low vibrational excitation observed for the FH product, as a result of the compensation between the effects of the reaction path curvature and the randomization of the energy favored by the deep hydrogen-bonded well. Variational transition state theory was used to calculate the rate constants for the title reaction and the kinetic isotope effects over the temperature range 100−500 K, finding that anharmonic effects are very important: they lower the rate constants by a factor of about 200 and make the agreement between our theoretical values and the experimental estimates reasonable. Finally, our results were compared with those obtained by means of the simple Gorin model that yields values very close to the experimental measurements.

Introduction

The title reaction is difficult to study experimentally, because it is a fast reaction followed by the extremely fast secondary atom/radical reaction $F + NH_2 \rightarrow FH + NH$, which is hard to eliminate by conventional experimental techniques. The title reaction has been widely studied by several experimental techniques,[1−9] and it yields a cold (noninverted) vibrational distribution of the FH product, although discrepancies have been found in the past, probably due to the experimental difficulties. Sloan et al.[6,8,9] have suggested that this cold, noninverted vibrational distribution could be caused by a strongly hydrogen-bonded $FH\cdots NH_2$ complex in the exit channel, which causes a randomization of the reaction exoergicity among all available product degrees of freedom. This behavior has been found in similar atom/radical reactions, such as[10] $F + HO \rightarrow FH + O$ and[11] $F + HCO \rightarrow FH + CO$, which present a deep well in the exit channel corresponding to a strongly bound intermediate. The rate constants also present large discrepancies with values ranging from 10^{-10} to 10^{-12} cm^3 molecule^{-1} s^{-1} at room temperature,[7,12−14] although few studies have been made.

The extensive experimental literature on this reaction contrasts with the paucity of theoretical studies, of which, to the best of our knowledge, there have been only two reported. In the first, Leroy et al.[15] studied the reaction using the ab initio UHF/6-31G level, with energy properties computed at the configuration interaction level. In the second, Goddard et al.,[8] using high-level ab initio calculations (up to 6-311G** CISD) found a hydrogen-bonded complex, $FH\cdots NH_2$, in the exit channel which is 8.1 kcal mol^{-1} more stable than the products. They suggested that this strong interaction will lead to fast internal vibrational relaxation of the exoergicity of the reaction, yielding a cold, noninverted, FH vibrational distribution. These theoretical works only studied the reactants, products, and complex properties, and the computational efforts to locate a saddle point were unsuccessful. Moreover, neither the reaction path nor the theoretical rate constants were calculated.

The deuterated analogue reaction, $ND_3 + F \rightarrow ND_2 + F$, has not been theoretically studied at all, and the few experimental measurements present contradictory results.[4,5,7,9] Thus, while Wategaonkar and Setser[7] found an inverted FD vibrational distribution, Donaldson et al.[5] found a hot (but noninverted) distribution, although these authors recognized a problem with their ND_3 data because the $ND_3 + F$ distribution is partly contaminated by a contribution from the secondary $ND_2 + F$ reaction, which produces an inverted FD distribution.

These practically barrierless hydrogen abstraction reactions are an exciting challenge for theoretical calculations, and since there is experimental interest in them, we have carried out a broad theoretical study of the reaction path to try to explain the product (FH/FD) vibrational distribution and to determine their rate constants using variational transition state theory .

Methods and Calculation Details

1. Calibration of the Analytical Potential Energy Surface Function. The first step in our calculation was to obtain an analytical expression for the potential energy surface (PES) of this reaction. Since the complete construction of an analytical PES for a polyatomic reaction is an arduous task, we used the same methodology employed in previous work for developing analytical PES's for polyatomic reactions,[16,17] based on modifying the analytical PES proposed for a similar reaction. We therefore changed some parameters of our recently proposed analytical PES for the $NH_3 + H \rightarrow NH_2 + H_2$ reaction.[18] We changed the parameters related to the geometric, energy and vibrational properties of the reactants and products, so that the exothermicity, geometries, and vibrational frequencies agreed reasonably well with the available experimental values.[19] The results of this fit are listed in Table 1.

In previous work,[16−18] the following step was to refit some parameters in order to reproduce the characteristics of an ab

* Author to whom correspondence should be addressed.
[⊗] Abstract published in *Advance ACS Abstracts,* May 15, 1997.

S1089-5639(97)00234-X CCC: $14.00

TABLE 1: Reactant and Product Properties[a] Calculated using the Analytical Surface

system	R_{NH}	R_{FH}	$\angle_{HNH}$	freq	V_{MEP}[b]	$\Delta H(0K)$[c]
reactants						
NH_3[d]	1.012		106.7	3542, 3433, 1702, 999	0.00	0.00
F						
products						
NH_2[e]	1.012		103.4	3205, 3164, 1508	−25.80	−29.95
FH[f]		0.917		4140		

[a] Distances in Å, angles in degrees, frequencies in cm^{-1}, and energies in kcal/mol. [b] Potential energy measured from reactants. [c] Measured from reactants. Experimental value:[19] −28.14 kcal/mol. [d] Experimental values:[19] R_{NH}, 1.012 Å; $\angle_{HNH}$, 106.7°; frequencies, 3577, 3506, 1691, 1022 cm^{-1}. [e] Experimental value:[19] R_{NH}, 1.024 Å; $\angle_{HNH}$, 103.4°; frequencies, 3220, 3173, 1497 cm^{-1}. [f] Experimental values:[19] R_{FH}, 0.917 Å; frequency, 4139 cm^{-1}.

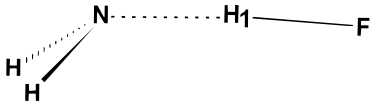

Figure 1. Hydrogen-bonded complex structure.

TABLE 2: Hydrogen-Bonded Complex Properties[a]

	analytical surface	ab initio calculations	
R_{NH1}	1.409	1.789[b]	1.816[c]
R_{NH}	1.013	1.021	1.020
R_{FH}	0.927	0.929	0.936
$\angle_{FH1N}$	175.8	180.0	180.0
$\angle_{HNH1}$	108.7	127.4	127.5
$\angle_{HNH}$	105.7	105.2	105.4
$V_{MEP,R}$[d]	−32.05	−34.2	−34.57
$V_{MEP,P}$[e]	−6.25	−11.1	−10.23
$\Delta H(0K)_R$[d]	−32.88	−34.9	−35.66
$\Delta H(0K)_P$[e]	−2.92	−6.7	−7.44
freq	3771, 3397, 3338, 1610, 978, 806, 230, 214, 195	3890, 3607, 3500, 1548, 832, 786, 284, 247, 193	3856, 3648, 3529, 1555, 774, 740, 274, 231, 174

[a] Distances in angles in degrees, frequencies in cm^{-1}, and energies in kcal/mol. Geometry according to Figure 1. [b] MP2/6-311G(d,p) optimized values.[8] [c] QCISD(T)/6-31++G(2d,p) energies and MP2/6-31G(d,p) geometries (this work). [d] Measured with respect to reactants. [e] Measured with respect to products.

TABLE 3: Refitted Parameters for the Analytical PES

param[a]	value	param[a]	value
$^3D_{NH}$	29.00 kcal mol^{-1}	α_{FH}	2.2180 $Å^{-1}$
$R_{FH}°$	0.9170 Å	$R_{NF}°$	1.4300 Å
$^1D_{FH}$	141.24 kcal mol^{-1}	$^1D_{NF}$	90.00 kcal mol^{-1}
$^3D_{FH}$	38.00 kcal mol^{-1}	$^3D_{NF}$	23.00 kcal mol^{-1}

[a] For a complete definition of the parameters and the analytical form of the PES, see ref 18.

initio calculated saddle point. Nevertheless, for this reaction, our attempts to find a saddle point by means of ab initio calculations were unsuccessful. The idea of this reaction occurring without a saddle point is supported by the large rate constants estimated experimentally and its large exothermicity. Since we need some reference information along the reaction path to fit some parameters of our new surface, we took as reference data the absence of saddle point and the properties of a stationary point found on the reaction path: the hydrogen-bonded complex linking the HF molecule and the NH_2 radical (Figure 1). The characteristics of this complex compared with the results found in the literature are listed in Table 2. Table 3 lists the parameters of our new surface which are different from the $NH_3 + H$ parameters. It should be noted that our fit was directed at obtaining a model analytical PES, rather than simply an accurate reproduction of the available experimental and theoretical values.

Once the analytical PES had been constructed (functional form and fitting procedure), the well formed by the hydrogen-bonded complex caused a serious problem in calculating the reaction path as a continuous path from reactants to products, because, being a stationary point, its first energy derivative with respect to the nuclear coordinates (gradient) is zero, causing a discontinuity. To solve this problem, the calculation of the reaction path was divided into two zones: the reactant and the product zones. In the reactant zone, we calculated the reaction path, starting by using a local cubic approach[20] from reactants separated by several distances, up to 9 Å, and going down the steepest descent path, using the Page and McIver method,[20,21] until we came close to the well. Since the well is a stationary point, the gradients along the reaction path become very small as we approach it, causing instabilities in the methods used for the reaction path calculation. Nevertheless, the properties of the last calculated points along the reaction path showed us that it leads from reactants to the hydrogen-bonded well.

To calculate the zone of the reaction path leading from this minimum to the products, we started a new calculation from products separated by up to 9 Å, going downhill to the complex until the gradients no longer allowed us to continue the calculation. Once again, the properties of the last points calculated along the reaction path were almost the same as those of the well, confirming that our reaction path leads from reactants to products via a hydrogen-bonded system.

Several trials were made with reaction paths starting from different distances between reactants or products. The final results in this paper are independent of increasing the starting distance further.

For a reaction path without a saddle point, the usual reaction coordinate, s, has arbitrary origin.[22] We choose the N−F distance as our reaction coordinate, since it behaves almost linearly, going to infinity at the reactants or products and reaching its minimum value in the region of the complex.

2. Computational Details. Once we had identified the reaction path, we used the Hessian matrix calculated at several points along the reaction path to perform a normal mode analysis. Following the reaction path Hamiltonian approach,[23] seven degrees of freedom from the calculated Hessian matrix were projected out, three corresponding to translational motion, three to rotational motion, and one to the reaction coordinate (which is not projected out at the stationary points). Therefore, along the reaction path we had eight frequencies, while at the stationary point we had nine.

These Hessian matrices also allowed us to compute the coupling terms B_{mF}, measuring the coupling between the normal mode m and the motion along the reaction coordinate F, and the Corioli-like term $B_{mm'}$, measuring the coupling between the normal modes m and m'. The B_{mF} coupling terms are the components of the reaction path curvature, $\kappa(s)$, defined as

$$\kappa(s) = \{\sum_m [B_{mF}(s)]^2\}^{1/2} \quad (1)$$

The interest in the calculation of these coupling terms lies in the qualitative explanation of the vibrational excitation experimentally observed in the FH/FD stretching mode in the products, and the comparison between the results obtained for the reactions of fluorine with both protonated and deuterated ammonia.

The knowledge of energies, vibrational frequencies, geometries, and gradients along the minimum energy path (MEP, taken as our reaction path) was used to estimate rate constants

by using variational transition state theory. The simplest variational method for the calculation of rate constants is the canonical approach (CVT).[24] In this, the location of the optimum transition state is given by the variation of the free energy of activation, $\Delta G(T,s)$, for a given temperature, T. The optimum transition state will depend only on the temperature, and it will be located at the maximum of $\Delta G(T,s)$, $\Delta G(T,s^*_{CVT})$. The rate constant will be given by

$$k^{CVT}(T) = \sigma\frac{kT}{h}K^\circ \exp[-\Delta G(T,s^*_{CVT})/kT] \qquad (2)$$

s^*_{CVT} being the location of the canonical transition state on the reaction path, k the Boltzmann constant, h the Planck constant, σ the symmetry factor (the number of equivalent reaction paths), and K° the reciprocal of the standard-state concentration, taken as 1 molecule cm^{-3}. The CVT approach has the problem that the effective threshold for a temperature may be lower than the maximum of the threshold at 0 K,[25] given by the maximum of the vibrationally adiabatic ground-state curve, $V_a^G(s)$, defined as

$$V_a^G(s) = V_{MEP}(s) + \epsilon^G_{vib}(s) \qquad (3)$$

where $V_{MEP}(s)$ stands for the energy along the MEP and $\epsilon^G_{vib}(s)$ is the vibrational zero-point energy for the ground state at s. To correct this threshold problem, the classical adiabatic ground-state (CAG) factor has been proposed, given by[24,25]

$$\kappa^{CVT/CAG}(T) = \exp\{-[V^{AG} - V_a^G(s^*_{CVT})]/kT\} \qquad (4)$$

V^{AG} being the maximum of the $V_a^G(s)$ curve. The corrected CVT/CAG rate constants are obtained by multiplying the k^{CVT} rate constant by the corresponding κ^{CAG} factor.

Obviously, a better method of correcting this problem would be a microcanonical calculation. The microcanonical variational rate constant, μVT, is calculated by locating the transition state for each energy and averaging the probabilities obtained using these transition states for a given temperature.[24,25] The cost in computer time for this kind of calculation is much larger than for CVT calculations, and the method will not be used in this paper.

An intermediate solution is to treat the probabilities for energies below the V^{AG} threshold microcanonically and the energies above it canonically. This approach leads to the improved CVT rate constant (ICVT),[24,25] which is only slightly more expensive computationally than a CVT calculation and gives a more reasonable correction for the problems of the canonical approximation than the CAG factor.

For hydrogen abstraction reactions the quantum tunneling effect is usually very important for an accurate rate constant calculation. Nevertheless, for reactions with low barrier heights or no saddle point, tunneling is negligible, if it exists at all. In all of our calculations we checked the importance of tunneling by computing it using zero or small curvature approximations[24] and found that the rate constants did not change by more than 10% in any case, even at very low temperatures where this effect is more important. Therefore, in all the results presented in this work, we neglect tunneling; i.e., we treat the motion along the reaction coordinate classically.

For the calculation of rotational partition functions we also used the classical approach. Even though some of the temperatures studied are quite low, we assume that this is still a good approximation, as we did in previous work where we checked its influence.[16,26] In order to take the spin−orbit effects into account, we included the $^2P_{1/2}$ state of the fluorine atom, 404 cm^{-1} higher than the $^2P_{3/2}$ ground state, in the electronic partition function of the reactants.[19] The points along the reaction path are assumed to have only one accessible electron state with a degeneracy of 2. In some cases, as discussed below, we included anharmonic effects in vibrational partition functions, using the mixed quadratic−quartic model.[27]

A very different approach to computing rate constants for reactions without a saddle point is to use Gorin's model.[22,28,29] This simple model is based on an attractive potential energy surface, with the analytical form

$$V_{MEP} = -C_6/R^6 \qquad (5)$$

where R(N−F) is the distance between the two approaching subsystems and C_6 is a constant calculated as

$$C_6 = C_{disp} + C_{ind} \qquad (6)$$

the dispersion term being

$$C_{disp} = \frac{3e^2\hbar^2}{2m_e}\frac{\alpha_A\alpha_B}{(\alpha_A/N_A)^{1/2} + (\alpha_B/N_B)^{1/2}} \qquad (7)$$

and the induction term

$$C_{ind} = d_B{}^2\alpha_A \qquad (8)$$

and α_X, N_X, and d_X being the polarizability, number of valence electrons, and dipole moment of the X subsystem, e and m_e the electronic charge and mass, all respectively, and $\hbar$ the Planck constant divided by 2π.

This model assumes that the dynamic bottleneck is located in the region where centrifugal and attractive forces in the complex formed by the two linked subsystems balance out. If the distance between the reactants is less than the equilibrium distance, the reaction occurs. Assuming free rotation and unperturbed vibration at the dynamic bottleneck (i.e., in the transition state, the vibrational properties are the same as for the reactants), the rate constant for overcoming the centrifugal barrier maximum when the two subsystems are different is given by[29,30]

$$k^{Gorin}(T) = \left(\frac{Q^{\ddagger}_{el}}{Q^{R}_{el}}\right)(\pi/\mu)^{1/2}(2kT)^{1/6}\Gamma(2/3)C_6{}^{1/3} \qquad (9)$$

where $Q^{\ddagger}_{el}$ and Q^{R}_{el} are the transition state and reactants electronic partition functions, μ is the reduced mass of the global system, and $\Gamma(x)$ is the incomplete Γ function.

Results and Discussion

1. Energy and Vibrational Properties. As mentioned above, the reaction coordinate is the distance between nitrogen and fluorine, which diminishes as one moves from reactants at an infinite separation to the complex, increasing again as one moves from the complex to the infinitely separated products. The variation of V_{MEP} (R_{N-F}) is shown in Figure 2. The discontinuity reflects the fact that we could not follow the reaction path continuously due to the zero gradients at the well. As the reactants approach one another, the potential energy diminishes slowly as a consequence of weak long-range attractive forces appearing. When the distance R_{N-F} reaches about 2.4 Å, the interaction becomes stronger and the change in energy is faster, falling more than 20 kcal/mol with a change in R_{N-F} smaller than 0.1 Å, and reaching the well. Since the bound molecules are the products of the reaction, we can

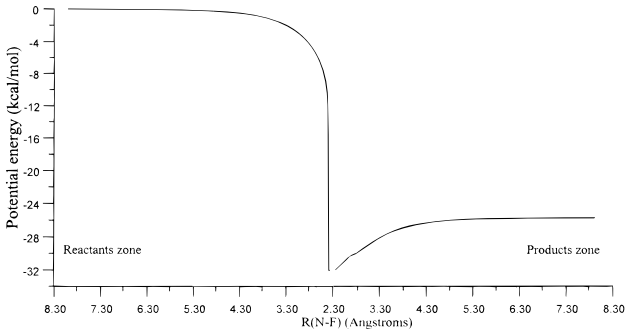

Figure 2. Potential energy surface along the reaction path plotted against the distance between N and F.

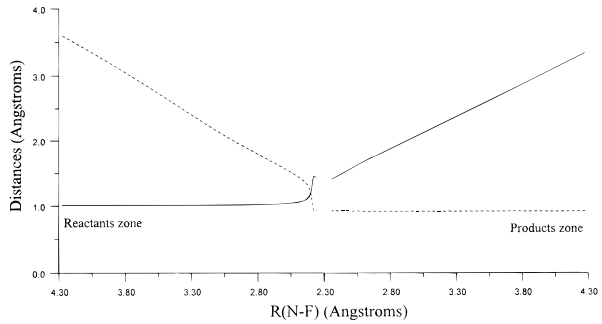

Figure 3. Variation of the $N-H_1$ (continuous line) and $F-H_1$ (dashed line) distances along the reaction path.

suppose that the hydrogen transfer occurs in a region close to the fall in V_{MEP}, since, if it happened in the flat region of small interactions, the breaking of the N−H bond would probably cause a saddle point. This will be examined below in more detail. After reaching the well, as the products start to separate, the energy increases again until it reaches a new flat region, where the long-range interactions keep the energy below its asymptotic product limit. The variation of $V_a^G(R_{N-F})$ presents behavior similar to that of V_{MEP}, and it is not shown in Figure 2.

The variation of the distances between the nitrogen and the hydrogen being transferred (R_{N-H}, solid line), and between this hydrogen and the fluorine atom (R_{F-H}, dashed line) are shown in Figure 3. Their behavior is similar to the trends in the energy: R_{N-H} is almost constant until the region around 2.4 Å is reached. Then, it increases rapidly, reaching a value near the one at the well ($R_{N-F} \cong 2.35$ Å). At this point, R_{F-H} also has a value very close to the one at the complex. This lends confidence to our earlier supposition about the location of the hydrogen transfer taking place in this area where the change in the energy is large.

The behavior of the harmonic frequencies along the reaction path is shown in Figure 4. For a clearer analysis, the vibrational modes are classified into three types:

(a) Spectator Modes. These modes are related to motions which are not directly involved in the reaction. For example, the two stretching modes in ammonia which change into stretching modes in the amidogen radical without changing their frequencies significantly. We will also consider as spectator modes two bending modes in ammonia, although one of them disappears as we advance from reactants to products, as well as the umbrella mode of ammonia.

(b) Transitional Modes. These modes appear along the reaction path as a consequence of the transformation of free rotations or free translations at the reactant or product limits into real vibrational motions in the global system. Their frequencies tend asymptotically to zero as R_{N-F} increases and

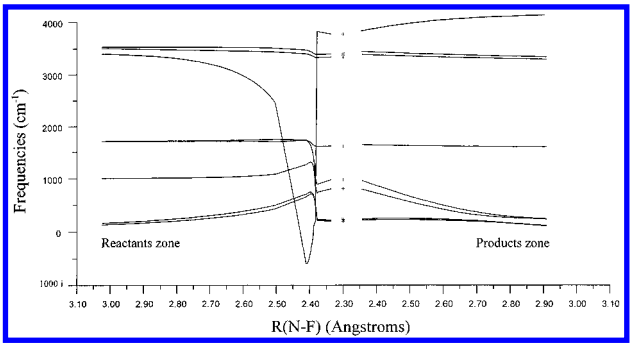

Figure 4. Harmonic frequencies along the reaction path. Asterisks indicate the values at the well.

reach their maxima near the well and before it. For this reaction, there are two transitional modes, which can be classified as bending along the N−H−F axis, having the lowest frequencies.

(c) Reactive Mode. This mode is directly involved in the hydrogen transfer and corresponds to an N−H stretching mode at the reactants, evolving to the F−H stretching mode at the products. Because of the breaking of the N−H bond, this frequency has a gradual but steady fall as we approach the transfer region, reaching imaginary values. As the transfer takes place, the forming of the F−H bond again increases the harmonic frequency of this mode very quickly, up to a value very close to its value at the complex. This mode suffers the most spectacular change in its frequency, which passes from 3542 cm^{-1} to about 600*i* cm^{-1} at a distance R_{N-F} of 2.38 Å in the reactant zone, and increasing again to 3820 cm^{-1} at 2.35 Å. Such a fast change and deep fall is typical of reactions such as the present having the heavy−light−heavy mass combination. Another noticeable factor in the analysis of this frequency is its value at the well, 369 cm^{-1} lower than its value at the separated products. This behavior is typical of systems linked by a hydrogen bond.

It is an undesired result to have an imaginary frequency after projecting out the seven degrees of freedom mentioned above. We can find imaginary frequencies for transitional modes in earlier works,[16−18,26,31−33] but this is the first time they have been found for the reactive mode. The possible causes of these unexpected values were looked at. There was no instability or lack of convergence on the calculated reaction path; and the use of curvilinear coordinates instead of the unphysical Cartesian coordinates, which was the solution in previous similar problems,[18,31,33] did not change the results at all. Whatever the reason, even though this is the region where the transfer occurs, it is not involved in our rate constant calculation (see below), and we think that the appearance of this imaginary frequency is not an important problem in our study.

In order to explain the vibrational excitation observed experimentally in the FH stretching, the coupling terms B_{mF} between the reaction coordinate and the vibrational modes were calculated. Figure 5 shows the total curvature term, $\kappa(s)$, for the most interesting zone: the transfer region. There are two regions where $\kappa(s)$ peaks: at 2.38 and 2.35 Å. The first maximum coincides with the fall of the reactive mode, while the second, which is very sharp and reaches a very high value, is located at the rise of this mode. An analysis of the curvature components at this second maximum shows that, although the bending ammonia modes contribute significantly to $\kappa(s)$, the mode exhibiting the largest coupling is the reactive mode, with a contribution over 5 times greater than the next most important contribution. From this behavior a large energy transfer from the reaction coordinate to the reactive mode can be expected, leading to a high vibrational excitation of the FH product.

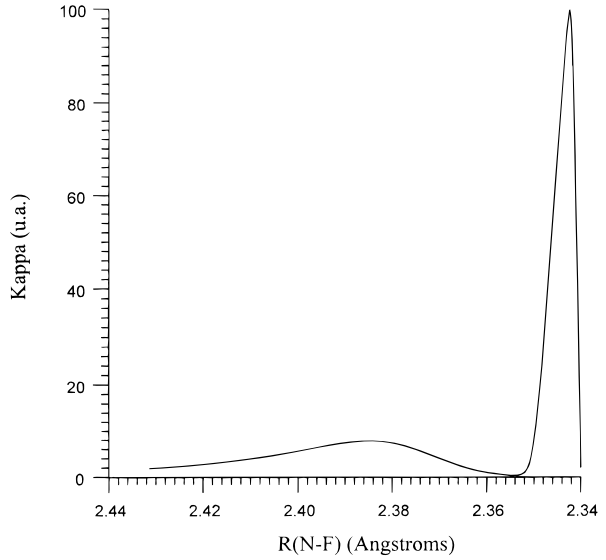

Figure 5. Reaction path curvature, κ, versus the N−F distance in the transfer region. For the sake of clarity, the highest peak has been truncated.

However, the experimentally observed vibrational excitation is smaller than in some other less exothermic reactions. Explanation of this experimentally observed fact has been based on the presence of the hydrogen-bonded complex.[8,9] The translational energy is nonadiabatically transferred to the forming FH bond, leading to excitation of the stretching mode. However, because of the stability of the complex formed, the system remains in the hydrogen-bonded situation for a certain time before evolving to the separated products. In this short lifetime of the bonded complex, there is a transfer of energy from the FH stretching mode to several other modes, especially the bending modes from ammonia, diminishing the FH excitation. When the system finally escapes from the well, this randomization of the energy has lead to an FH excitation which is smaller than in other direct reactions without the possibility of such an effective randomization.

In order to test this hypothesis, we calculated the coupling between the vibrational modes, $B_{mm'}$, near the complex. Although several modes seem to be coupled in the region of the higher $\kappa(s)$ peak, two $B_{mm'}$ terms are especially larger: those that measure the coupling between the reactive mode and the ammonia bending modes (Figure 6). Therefore, while the system continues as the bonded complex, the translational energy, now stored in the FH stretching, is randomized, going especially to the ammonia bendings. When the system finally reaches the products, the translational energy is distributed between the FH stretching, the NH_2 bending, and rotational or translational energy (as a consequence of the energy of the transitional modes disappearing and the ammonia bending and umbrella modes), explaining the low final FH excitation.

We will now examine the behavior of the deuterated ammonia isotopomer, where there exist experimental doubts about the vibrational distribution. While Wategaonkar and Setser[7] found an inverted distribution, Donaldson et al.[5] found a strongly inverted distribution at high reagent flows and a noninverted distribution (although hot) at low reagent flows. Obviously, there is no difference in the energy description of the two isotopomers, since both are based on the same Born−Oppenheimer PES. The only differences appear when the vibrational study is included. Table 4 lists the energy including zero-point energy effects (i.e., $\Delta H(0K)$ or differences in V_a^G) for both the protonated and deuterated systems and Table 5 the vibrational frequencies at the deuterated stationary points.

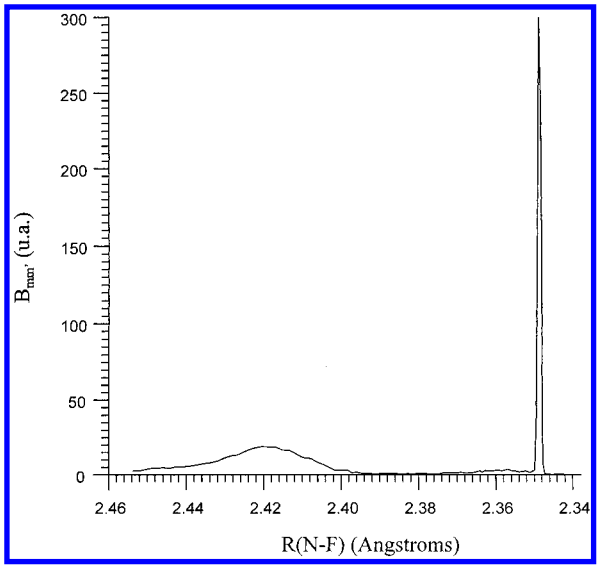

Figure 6. Corioli coupling term, $B_{mm'}$, between one ammonia bending mode and the reactive mode, in the transfer region. For the sake of clarity, the highest peak has been truncated.

TABLE 4: V_{MEP} and $\Delta H(0K)$ for the Complex for Both Isotopic Reactions[a]

	$NH_3 + F$	$ND_3 + F$
$V_{MEP,R}$[b]	−32.05	
$V_{MEP,P}$[c]	−6.25	
$\Delta H(0K)_R$[d]	−32.88	−32.59
$\Delta H(0K)_p$[e]	−2.92	−3.71

[a] Energies in kcal/mol. [b] Potential energy referred to reactants. [c] Potential energy referred to products. [d] Enthalpy at 0 K referred to reactants. [e] Enthalpy at 0 K referred to products.

TABLE 5: Frequencies for the Deuterated Stationary Points[a]

system	freq	system	freq
ND_3[b]	2618, 2463, 1230, 756	complex	2737, 2504, 2426, 1176,
ND_2[c]	2358, 2303, 1100		707, 615, 218, 154, 140
FD[d]	3001		

[a] In cm^{-1}. [b] Experimental values:[19] 2618, 2463, 1230, 756. [c] Experimental values:[19] 2367, 2305, 1110. [d] Experimental value:[19] 3001.

The changes in harmonic frequencies and curvature terms, $\kappa(s)$, B_{mF}, and $B_{mm'}$ are very similar to those observed for the protonated system and will not be shown here. Again, the reactive mode shows a large fall in frequency, from over 2600 to 260*i* cm^{-1}, and then increasing again until it reaches its value at the well, over 2700 cm^{-1}. This similarity in behavior indicates that our previous discussion concerning the transfer of translational energy to the reactive mode and later randomization into the other modes must be also applicable here.

With this information, the experimental differences between the protonated and the deuterated analogues can be explained. In the translational−vibrational energy transfer, there are two opposing effects. On the one hand, since the vibrational excitation of FD requires less energy than the FH excitation (according to the harmonic approximation, about 38% less for the deuterated well), it seems logical to suppose that the FD product will have a higher vibrational population in its excited states than the FH product. On the other hand, if we analyze Table 4, the well in the deuterated reaction is slightly deeper with respect to the products than in the protonated case (0.79 kcal mol^{-1} deeper), so that the time for randomization should be longer and, as a consequence, there should be a greater loss of vibrational energy from the FD stretching mode. Quantita-

TABLE 6: Rate Constants and Kinetic Isotope Effects for the $NH_3 + F$ Reaction

	CVT		CVT/CAG		ICVT	
T (K)	k^a	KIE^b	k	KIE	k	KIE
100	5.03×10^{-9}	1.15	9.41×10^{-10}	1.00	4.44×10^{-9}	1.09
200	3.30×10^{-9}	0.89	4.84×10^{-10}	0.63	2.73×10^{-9}	0.79
298	2.36×10^{-9}	0.75	3.15×10^{-10}	0.57	1.84×10^{-9}	0.80
400	1.77×10^{-9}	0.69	2.05×10^{-10}	0.74	1.26×10^{-9}	0.85
500	1.36×10^{-9}	0.76	1.33×10^{-10}	1.65	9.52×10^{-10}	0.88

[a] In cm^3 molecule^{-1} s^{-1}. Experimental values at 298 K: 1.09×10^{-10},[7] 1.19×10^{-10},[14] 3.9×10^{-11},[13] 9.13×10^{-13}.[12] [b] Defined as $k(NH_3)/k(ND_3)$. Experimental value at 298 K:[7] 1.1 ± 0.2.

tively, the former factor seems to be more important than the latter, and the FD product will have a higher vibrational population in its excited state than the FH, in agreement with the experimental results.[4−7,9]

2. Rate Constants and Kinetic Isotope Effects. The rate constants for both the protonated and deuterated isotopes of ammonia were calculated using CVT, CVT/CAG, and ICVT methods, using the harmonic model for the vibrational partition functions and treating rotations and translation along the reaction path classically. Table 6 lists the rate constants and the kinetic isotope effects (KIE's) estimated using the three vibrational approximations in the temperature range 100−500 K.

The first noteworthy observation is the importance of the CAG factor (between 0.09 and 0.19). In order to clarify the reasons for this, Table 7 lists the location of the canonical transition state for the calculated temperatures and its most important properties. Since the potential energy along the reaction path diminishes continuously and the frequencies along it change very slowly in the region previous to the abrupt change in V_{MEP}, the V_a^G curve follows the same trend as V_{MEP}, reaching its maximum, V^{AG}, at the reactants. However, as can be seen in Table 7, as the temperature rises, the canonical transition states shift away from the reactants. This is because their location is the result of attempting to avoid low values of the frequencies of the transitional modes (which, under harmonic approaches, would in turn lead to extremely low values of ΔG). As a consequence, κ^{CAG}, which decreases as the difference between V^{AG} and $V_a^G(s^*_{CVT})$ increases, is very different from unity. This is due to that CVT/CAG is based on the ground state and will become inaccurate at high temperature. The physical meaning of this is that, since the canonical transition state is located at a point with V_a^G lower than V^{AG}, the CVT rate constant is considering as reactive a great many trajectories with energy less than V^{AG} which are classically unreactive. Nevertheless, such a large correction to eliminate those trajectories seems to be overestimating their importance, but neglecting them (i.e., considering κ^{CAG} as unity) would probably cause an overestimate of the rate constant. We therefore considered the ICVT rate constants as the most accurate of those calculated here. As a test, we made some microcanonical calculations in order to check the deviations from the correct treatment of the ICVT-calculated thresholds, finding differences of less than 30% between the ICVT and μCVT rate constants for the protonated system.

Yet with this ICVT approach the computed rate constants at room temperature are larger than the experimental values. In order to find the possible reasons for this overestimate, several sources of error were checked:

(a) Deficiencies of the PES. This is the most obvious source of errors. The unavailability of ab initio data about the reaction path makes it impossible to check it more deeply. However, on the basis of our experience with similar reactions,[16−18,33] we would assume that this PES is suitable for the present calculations, taking into account the semiempirical nature of this surface and, therefore, that the reason for the deviations from experiment lies elsewhere.

(b) Recrossing across the Transition States. Transition state theory assumes that recrossing across the canonical transition states is negligible, leading to an overestimate of the computed rate constants. The importance of recrossing effects can only be determined by means of quantum scattering calculations, trajectory calculations, dynamics studies, etc., all of which lie beyond the scope of this work. Part of the recrossing effects for a reaction path with two ΔG maxima, as is the present case (one between reactants and well and another between well and products), can be eliminated using the unified statistical model (US).[24] Under a canonical approach (CUS), we can write

$$k^{CUS}(T) = k^{CVT}(T)\, R^{CUS}(T) \tag{10}$$

with

$$R^{CUS}(T) = \left[1 + \frac{k^{CVT}}{k^{max}} + \frac{k^{CVT}}{k^{min}}\right]^{-1} \tag{11}$$

where k^{CVT} is calculated at the highest maximum of ΔG, k^{max} at the second highest maximum, and k^{min} at the minimum of ΔG, measured from the reactants. Since the second highest maximum of ΔG is located at the product channel, the barrier height is around −25 kcal/mol. Therefore the rate constant k^{max} can be expected to be much larger than k^{CVT}. A rate constant calculation confirmed this point. Moreover, following the same idea, k^{min}, which has to be larger than k^{max}, will also be much larger than k^{CVT}. The fractions in R^{CUS} will thus be close to zero, $R^{CUS} = 1$ and $k^{CUS} = k^{CVT}$. The recrossing effects, according to the CUS correction, are, therefore, negligible in this reaction.

(c) Anharmonicity. As we mentioned before, the most important factor in the location of the canonical transition states is presented by the frequencies of the transitional modes, since when they have low values, the partition functions are very large

TABLE 7: Selected Properties[a] of the CVT and ICVT Transition States

T (K)	method	R_{NF}	R_{NH}	R_{FH}	V_{MEP}	freq
100	CVT	4.470	1.012	3.555	−0.39	3542, 3541, 3432, 1702, 1702, 999, 19, 19
	ICVT	4.259	1.012	3.339	−0.52	3542, 3541, 3432, 1702, 1702, 998, 24, 24
200	CVT	3.919	1.012	2.980	−0.85	3541, 3540, 3431, 1702, 1702, 998, 39, 37
	ICVT	3.633	1.012	2.672	−1.28	3541, 3538, 3429, 1703, 1702, 997, 58, 52
298	CVT	3.607	1.012	2.644	−1.33	3541, 3537, 3428, 1703, 1702, 997, 60, 54
	ICVT	3.141	1.013	2.144	−2.60	3538, 3521, 3414, 1706, 1703, 996, 125, 106
400	CVT	3.348	1.012	2.365	−1.93	3539, 3532, 3424, 1704, 1703, 996, 89, 77
	ICVT	2.907	1.016	1.898	−3.68	3534, 3494, 3373, 1710, 1704, 1000, 192, 161
500	CVT	3.141	1.013	2.144	−2.60	3.538, 3521, 3414, 1706, 1703, 996, 125, 106
	ICVT	2.829	1.017	1.817	−4.16	3532, 3482, 3336, 1712, 1704, 1004, 225, 188

[a] Distances in Å, energy in kcal mol^{-1}, and frequencies in cm^{-1}.

TABLE 8: Rate Constants and Kinetic Isotope Effects for the $NH_3 + F$ Reaction, Including Anharmonic Effects

	CVT		CVT/CAG		ICVT	
T (K)	k^a	KIE^b	k	KIE	k	KIE
100	6.32×10^{-13}	0.34	6.32×10^{-13}	0.34	6.32×10^{-13}	0.32
200	5.52×10^{-12}	0.65	4.35×10^{-12}	0.63	5.48×10^{-12}	0.65
298	1.06×10^{-11}	0.80	8.12×10^{-12}	0.77	1.05×10^{-11}	0.80
400	1.49×10^{-11}	0.87	1.13×10^{-11}	0.86	1.48×10^{-11}	0.87
500	1.84×10^{-11}	0.94	1.39×10^{-11}	1.36	1.83×10^{-11}	1.00

[a] In cm^3 molecule^{-1} s^{-1}. Experimental values at 298 K: 1.09×10^{-10},[7] 1.19×10^{-10},[14] 3.9×10^{-11},[13] 9.13×10^{-13}.[12] [b] Defined as $k(NH_3)/k(ND_3)$. Experimental value at 298 K:[7] 1.1 ± 0.2.

TABLE 9: Factor Analysis of the KIE's

T (K)	KIE	η_{trans}	$\eta_{rot.}$	η_{vib}	$\eta_{pot.}$
		Harmonic Approach			
100	1.15	1.13	1.73	0.47	1.25
200	0.89	1.13	1.65	0.31	1.58
298	0.75	1.13	1.71	0.30	1.29
400	0.69	1.13	1.79	0.32	1.07
500	0.76	1.13	2.00	0.66	0.51
		Anharmonic approach			
100	0.34	1.13	2.18	0.14	0.98
200	0.65	1.13	1.78	0.32	1.00
298	0.80	1.13	1.78	0.39	1.02
400	0.87	1.13	1.80	0.42	1.02
500	0.94	1.13	1.06	0.61	1.28

and ΔG is very small. The transition states are located at points where those frequencies are not very low and the fall in V_{MEP} is not yet very large. There were low values of the transitional mode frequencies (Table 7). Therefore, considerable anharmonic effects can be expected. To calculate the influence of anharmonicity, we computed the partition functions for transitional modes using the mixed quadratic−quartic approach.[27] The other modes were assumed to stay harmonic: since these modes are not very different in the transition state and, in the reactants, the anharmonic effects for these modes can be expected to cancel out when we calculate the rate constants. The anharmonic rate constants and the KIE's are shown in Table 8. The rate constants are lowered by a factor of about 200 at room temperature, so that the theoretical values are in the range of experimentally measured rate constants, although about 10 times lower than the most recent measurements.[7,14]

It is noticeable that the inclusion of anharmonicity involves an inversion in the dependence of the rate constants on the temperature. The reason is the increase in the activation energy, changing from -0.7 kcal mol^{-1} at 298−300 K under the harmonic approximation (negative dependence on the temperature) to $+0.7$ kcal mol^{-1} under the anharmonic approximation (positive dependence).

Another interesting factor is represented by the large differences between the calculated KIE's and their dependence on the temperature. Unfortunately, experimental information does not clarify the situation, since at the only measured temperature[7] the harmonic and anharmonic approximations give a similar result, 0.80, close to the experimental value, 1.1 ± 0.2. To analyze their behavior in more detail, in Table 9 we list the components of the KIEs for harmonic and anharmonic approaches, at the variational transition state. The NH_3/ND_3 KIE's factorize as[34]

$$\mathrm{KIE} = K_H/K_D = \eta_{trans}\eta_{rot.}\eta_{vib}\eta_{pot.} \qquad (12)$$

where η_{trans} is the ratio of the relative translational partition functions, $\eta_{rot.}$ is from rotation, η_{vib} is from vibration, and $\eta_{pot.}$ is from V_{MEP}. Note that the KIE's are defined as the ratio of NH_3 to ND_3 reactions rate constants. This follows the conventional approach in which the rate for the lighter isotopomer is always in the numerator. With this convention, KIE's greater than 1 are called "normal" and those less than 1 are called "inverse". From an examination of this table we see that the translational contribution is independent of temperature, and the $\eta_{rot.}$ and $\eta_{pot.}$ contributions practically cancel in the temperature range studied. Hence, almost all of the temperature dependence and the inverted behavior of the KIE's comes from the vibrational contribution. This η_{vib} explains the differences between the harmonic and anharmonic approaches. Thus, in the harmonic approach η_{vib} drops and then rises slightly with increasing temperature in parallel with the KIE's, while in the anharmonic approach the increase of the KIE's with temperature is caused by the rise of η_{vib}, with a more than 4-fold increase from 100 to 500 K.

TABLE 10: Selected Properties[a] of the CVT and ICVT Transition States Calculated using Anharmonic Partition Functions

T (K)	method	R_{NF}	R_{NH}	R_{FH}	V_{MEP}	freq[b]
100	CVT	6.310	1.012	5.302	−0.03	3, 1
	ICVT	6.310	1.012	5.302	−0.03	3, 1
200	CVT	5.400	1.012	4.449	−0.11	8, 7
	ICVT	5.347	1.012	4.400	−0.12	8, 8
298	CVT	5.080	1.012	4.150	−0.17	10, 10
	ICVT	5.027	1.012	4.100	−0.18	11, 11
400	CVT	4.841	1.012	3.922	−0.23	13, 13
	ICVT	4.788	1.012	3.870	−0.25	13, 14
500	CVT	4.655	1.012	3.740	−0.30	15, 16
	ICVT	4.602	1.012	3.688	−0.33	16, 17

[a] Distances in Å, energy in kcal mol^{-1}, and frequencies in cm^{-1}. [b] Transitional mode harmonic frequencies. The nonincluded frequencies are less than 1 cm^{-1} different in value than the reactant frequencies.

Table 10 shows the properties of the CVT and ICVT transition states for anharmonic calculations. The most remarkable fact is that the transition states are now closer to the reactants, since the partition functions are much smaller for low transitional frequencies than under the harmonic approach, allowing the location of the transition states to be at regions of higher V_{MEP}, larger values of R_{N-F} and lower transitional frequencies. As a consequence, V^{AG} is closer to $V_a^G(s^*_{CVT})$ and k^{CVT}, k^{ICVT}, and $k^{CVT/CAG}$ are closer than under the harmonic approximation.

The proximity of the transition states to the reactants may make our calculation of the electronic partition functions inaccurate, since transition states may have, as does the fluorine, two or more electronic states close in energy. In order to check the importance of this effect, the rate constants were recalculated including the same electronic states for the transition state as for fluorine (assuming that the transition states are so close to the reactants that they behave similarly from the electronic state point of view). The rate constants increased by a factor of about 2, this factor being the upper limit for the influence of this problem.

Since the transition states are so close to the reactants, we can suppose that Gorin's model, based on transition states located at the vibrationally unperturbed reactants, could be applicable to this reaction. Note that, while the transitional modes were the most important point in the previous calculations, i.e., the vibrational perturbation of the reactants, Gorin's model eliminates this contribution from the calculation, basing all of the kinetic factors on pure reactant properties. These are, therefore, two different (even opposite) approaches for the kinetic study of this reaction. Two methods were employed for the calculation of C_6: the usual calculation, following eqs 6 and 8 and neglecting C_{disp};[30] and fitting the potential from eq

TABLE 11: Rate Constants and Kinetic Isotope Effects for the $NH_3 + F$ Reaction Calculated using Gorin's Model

	$C_6 = 38.7$[a]		$C_6 = 149.2$	
T (K)	k[b]	KIE[c]	k	KIE
100	1.83×10^{-10}	1.04	2.87×10^{-10}	1.04
200	2.00×10^{-10}	1.04	3.14×10^{-10}	1.04
298	2.05×10^{-10}	1.04	3.22×10^{-10}	1.04
400	2.07×10^{-10}	1.04	3.24×10^{-10}	1.04
500	2.07×10^{-10}	1.04	3.25×10^{-10}	1.04

[a] In units of 10^{-60} erg cm^6. [b] In cm^3 molecule^{-1} s^{-1}. Experimental values at 298 K: 1.09×10^{-10},[7] 1.19×10^{-10},[14] 3.9×10^{-11},[13] 9.13×10^{-13}.[12] [c] Defined as $k(NH_3)/k(ND_3)$. Experimental value at 298 K:[7] 1.1 ± 0.2.

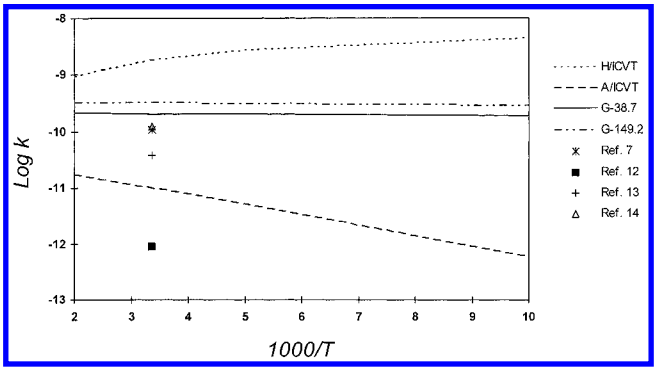

Figure 7. Arrhenius plot of $\log_{10} k$ (cm^3 molecule^{-1} s^{-1}) against the reciprocal temperature (K) of the rate constants calculated using different methods, and the experimentally measured rate constants: H/ICVT, harmonic ICVT rate constants; A/ICVT, anharmonic ICVT rate constants; G-38.7, Gorin's model rate constants computed using $C_6 = 38.7 \times 10^{-60}$ erg cm^6; G-149.2, Gorin's model rate constants computed using $C_6 = 149.2 \times 10^{-60}$ erg cm^6.

5 to reproduce the computed V_{MEP} for our analytical surface. The values of C_6 obtained are 38.7 and 149.2 in units of 10^{-60} erg cm^6 for each calculation method, respectively. Although these values for C_6 are very different, the rate constants only differ by a factor of 1.6, since they depend on the cube root of C_6. Table 11 lists the computed rate constants and KIE's calculated using this simple model.

Finally, Figure 7 shows the values of the rate constants obtained in this work using different approaches together with the experimental values. Two conclusions can be drawn from Figure 7 and Table 11. The first is that Gorin's model provides rate constants with an almost negligible dependence on temperature. The reason is that the only terms in which temperature appears are the electronic partition functions, which change very little with temperature, and the term $(2kT)^{1/6}$, which also shows little dependence. The second conclusion is that the KIE's are independent of the temperature. The only effect of an isotopic substitution on the rate constant is in the change in the reduced mass, affecting all of the temperatures in the same way. This is also independent of the C_6 factor.

The rate constants and KIE's calculated by means of Gorin's model are in surprisingly good agreement with the experimental results. Perhaps, given the simplicity of the model and of the approximations assumed, it is only a fortuitous agreement. But, since the transition states located using variational transition state theory are so close to the reactants, it seems that the foundation of Gorin's model is essentially correct for this reaction. Nevertheless, to check any of the present deductions concerning the kinetics of this reaction, a deeper experimental study of rate constants, KIE's and, especially, their dependence on the temperature will be advisable.

Conclusions

The gas phase $NH_3 + F$ reaction and its deuterated analogue were studied by means of an analytical PES. We demonstrated that there is a large vibrational excitation of the FH stretching mode due to the coupling between this mode and the reactive mode, but the excitation energy is randomized because of the large coupling between the reactive mode and the remaining modes and because of the time that the system exists as a hydrogen-bonded complex before evolving to separated NH_2 and FH. As a consequence, the FH stretching mode is less excited than in other direct reactions. We have also suggested that the larger excitation observed in the deuterated isotopic system can be explained in terms of the smaller energy requirements for the FD excitation than for the FH case.

From a kinetics point of view, using variational transition state theory, we found that anharmonicity is an extremely important factor, since the location of the transition states is given mainly by the transitional modes which are usually modes of very low frequencies and very anharmonic. Including anharmonicity changes the value of the rate constant at 298 K by a factor of about 200 and inverts the temperature dependence of the rate constants and KIE's, yielding good agreement with the scarce experimental results. The similarity between the transition states and reactants (especially when anharmonicity is included) makes the use of Gorin's model reasonable for computing the rate constants, obtaining values almost independent of the temperature, and KIE's which are constant with respect to the temperature and dependent only on the relative mass of the system. In spite of the simplicity of this model, it gives results closer to the most recent experimental measurements than the much more complicated variational transition state based methods.

Since no experimental result is available to shed any light on the question of the temperature dependence of the rate constants and KIE's, we think that experimentalists may be encouraged to study more deeply the kinetics of this very interesting and little known reaction, although we are aware of the very great experimental difficulty involved.

Acknowledgment. The authors would like to thank the Dirección General de Investigación Científica y Técnica del Ministerio de Educación y Ciencia for partial support of this work (Project PB94-1030). J.C.C. thanks Junta de Extremadura for a scholarship. We also thank Prof. Donald G. Truhlar for providing us with a copy of Polyrate 7.0.

References and Notes

(1) Duewer, W. H.; Setser, D. W. *J. Chem. Phys.* **1973**, *58*, 2310.
(2) Douglas, D. J.; Sloan, J. J. *Chem. Phys.* **1980**, *46*, 307.
(3) Sloan, J. J.; Watson, D. G.; Williamson, J. *Chem. Phys. Lett.* **1980**, *74*, 481.
(4) Manocha, D. S.; Setser, D. W.; Wickramaaratchi, M. *Chem. Phys.* **1983**, *76*, 129.
(5) Donaldson, D. J.; Parsons, J.; Solan, J. J.; Stolow, A. *Chem. Phys.* **1984**, *85*, 47.
(6) Donaldson, D. J.; Sloan, J. J.; Goddard, J. D. *J. Chem. Phys.* **1985**, *82*, 4524.
(7) Wategaonkar, S.; Setser, D. W. *J. Chem. Phys.* **1987**, *86*, 4477.
(8) Goddard, J. D.; Donaldson, D. J.; Sloan, J. J. *Chem. Phys.* **1987**, *114*, 321.
(9) Sloan, J. J. *J. Phys. Chem.* **1988**, *92*, 18.
(10) Sloan, J. J.; Watson, D. G.; Williamson, J. M.; Wright, J. S. *J. Chem. Phys.* **1981**, *75*, 1190.
(11) Donaldson, D. J.; Sloan, J. J. *J. Chem. Phys.* **1985**, *82*, 1873.
(12) Pollock, T. L.; Jones, W. E. *Can. J. Chem.* **1973**, *51*, 204.
(13) Houston, P. L. *Adv. Chem. Phys.* **1982**, *47*, 625.
(14) Fagerström, K.; Jodkowski, S. T.; Lund, A.; Ratajczak, E. *Chem. Phys. Lett.* **1995**, *236*, 103.
(15) Leroy, G.; Sana, M.; Tinant, A. *Can. J. Chem.* **1985**, *63*, 1447.

(16) Corchado, J. C.; Espinosa-García, J. *J. Chem. Phys.* **1996**, *105*, 3160.

(17) Espinosa-García, J.; Corchado, J. C. *J. Chem. Phys.* **1996**, *105*, 3517.

(18) Corchado, J. C.; Espinosa-García, J. *J. Chem. Phys*, in press.

(19) *JANAF Thermochemical Tables*, 3rd ed.: Chase, M. W., Jr., Davies, C. A., Downey, J. R., Jr., Frurip, D. J., McDonald, R. A., Syverud, A. N., Eds.; National Standard Reference Data Series, Vol. 14, National Bureau of Standards: Washington, DC, 1985.

(20) Page, M.; McIver, J. W., Jr. *J. Chem. Phys.* **1988**, *88*, 922.

(21) Page, M.; Doubleday, C.; McIver, J. W., Jr. *J. Chem. Phys.* **1990**, *93*, 5634.

(22) Rai, S. N.; Truhlar, D. G. *J. Chem. Phys.* **1983**, *79*, 6046.

(23) Miller, W. H.; Handy, N. C.; Adams, J. E. *J. Chem. Phys.* **1980**, *72*, 99.

(24) See, for example: Truhlar, D. G.; Isaacson, A. D.; Garrett, B. C. In *The Theory of Chemical Reactions*; Bear, M., Ed.; Chemical Rubber: Bocan Raton, FL, 1985; Vol. 4.

(25) Garrett, B. C.; Truhlar, D. G.; Grev, R. S.; Magnuson, A. W. *J. Phys. Chem.* **1980**, *84*, 1730.

(26) Corchado, J. C.; Espinosa-García, J. *J. Chem. Phys.* **1996**, *105*, 3152.

(27) Isaacson, A. D.; Truhlar, D. G. *J. Chem. Phys.* **1982**, *76*, 1380. Truhlar, D. G. *J. Mol. Spectrosc.* **1971**, *38*, 415. Garrett, B. C.; Truhlar, D. G. *J. Phys. Chem.* **1979**, *83*, 1915.

(28) Gorin, E. *Acta Physicochim. USSR* **1938**, *9*, 68.

(29) Garrett, B. C.; Truhlar, D. G. *J. Am. Chem. Soc.* **1979**, *101*, 4534.

(30) Johnston, H. S.; Goldfinger, P. *J. Chem. Phys.* **1962**, *37*, 700.

(31) Natanson, G. A.; Garrett, B. C.; Truong, T.; Joseph, T.; Truhlar, D. G. *J. Chem. Phys.* **1991**, *94*, 7875. Jackels, C. F.; Gu, Z.; Truhlar, D. G. *J. Chem. Phys.* **1995**, *102*, 3118.

(32) Soto, M. R.; Page, M. *J. Chem. Phys.* **1992**, *97*, 7287.

(33) Espinosa-García, J.; Corchado, J. C. *J. Phys. Chem.* **1996**, *100*, 16561.

(34) Garret, B. C.; Truhlar, D. G.; Magnuson, A. W. *J. Chem. Phys.* **1982**, *76*, 2321. Tucker, S. C.; Truhlar, D. G.; Garrett, B. C.; Isaacson, A. D. *J. Chem. Phys.* **1985**, *82*, 4102. Gonzalez-Lafont, A.; Truong, T. N.; Truhlar, D. G. *J. Phys. Chem.* **1991**, *95*, 4618.